Automated E-Field Scanning System for Dosimetric Assessments

Thomas Schmid, Oliver Egger, and Niels Kuster

Abstract— **The interest in accurate dosimetric measurements inside phantoms that simulate biological bodies has burgeoned since several regulatory commissions began calling for or recommending the testing for compliance with safety standards of low power devices. This paper presents a newly developed, robot-based system that allows automated E-field scanning in tissue simulating solutions. The distinguishing characteristics of the system are its high sensitivity and its broad dynamic range (1 μW/g to 100 mW/g) over the entire frequency range (10 MHz to over 3 GHz) used for mobile communications. The reproducibility of the dosimetric evaluations has been shown to be considerably better than ±5%. This has been accomplished by the use of an improved isotropic E-field probe connected to amplifiers with extremely low noise and drift characteristics in conjunction with digital processing of the data. Special emphasis has been placed on system reliability, user-friendliness and graphic visualization of data.**

I. Introduction

THE question of whether low power transceivers comply with current safety limits was first raised by Cleveland *et al.* [1]. Two years later the study of the absorption mechanism in the near field of sources revealed a direct contradiction of the exclusion clause for low power devices with basic safety restrictions [2]. Additional findings of the latter study relevant for this paper were:

1) In the close near field, induced currents are mainly caused by the inductive coupling of the high frequency (HF) current distribution on the radiating structure with the biological body.
2) The induced specific absorption rate (SAR) depends more on the actual design and the position of the radiating structure with respect to the body than on the inhomogeneity of the tissue.
3) Devices with an input power of considerably less than 1 W might violate the basic safety limits for partial body exposure which are: 1.6 mW/g averaged over 1 g (ANSI/IEEE [3]), 2.0 mW/g averaged over 10 g tissue (CENELEC [4]), respectively.

These findings have been confirmed in the following by studies with partially homogeneous bodies exposed to dipole and helix antennas [4], [6] and by a study with largely inhomogeneous head phantoms [7].

Several recently published dosimetric studies on current mobile phones found spatial peak SAR values in the range of the safety limits for uncontrolled environments [8]–[13]. Under certain conditions, these limits were exceeded [8], [10], [11], [13]. This caused some concern in the industry as the current trend towards miniaturization with shorter antennas is bound to lead to higher absorption if these issues are not carefully considered during the design process.

Taking various concerns and factors into consideration, individual type approval using dosimetric tests is the most sound approach for both the public as well as industry. As far back as 1992, the German Agency for Radiation Protection [14] recommended type approval for mobile communication devices. The FCC [15] has now taken a similar stance and is calling for the demonstration that the maximum SAR for PCS devices with output power of more than 100 mW complies with the ANSI/IEEE guidelines for SAR values.

Needless to say, such test procedures will lead to decisions with far-reaching economic consequences. It is therefore essential that the testing procedure meets the highest possible standards of accuracy, reproducibility, standardization, and availability during the design procedure of new devices. A critical issue is the operating position of the device being tested. In case compliance must be demonstrated for the use of the device under all operational conditions [14], it is not sufficient to test the device by measurement or computation in one particular predefined position (e.g., normal position). Instead, the "worst case" exposure situation among all operational conditions must be tested. This "worst case" exposure situation can only be determined by varying the most relevant parameters such as the position of the device, the operational condition of the device (e.g., extended or retracted antenna), use by left- or right-handers, variations of head shape, and the position of the hand holding the device.

As no system is yet available that satisfies all these requirements, several groups are currently engaged in developing numerical simulation tools or measurement systems for safety assessments of handheld transceivers.

Although anatomical details can now be represented with considerable detail, the numerical approach is fraught with serious difficulties. 1) As today's transceivers have been optimized with regard to size, weight and appearance, simple modelling of the transmitter as a metal box with antenna may not suffice, even if the geometry has been correctly discretized. The reason is that considerable HF currents may flow on internal substructures of the transceivers which, in turn, can induce high SAR values. The HF coupling mechanisms of these internal structures are often not obvious and it can therefore be difficult to arrive at the appropriate numerical

Manuscript received April 10, 1995; revised October 2, 1995.
The authors are with the Swiss Federal Institute of Technology, CH-8092, Zurich, Switzerland.
Publisher Item Identifier S 0018-9480(96)00464-4.

modelling. In addition, these effects can undergo considerable changes in the vicinity of the scatterer. 2) If compliance under all operational conditions is required, a number of simulations must be performed, which necessitate techniques that are efficient, largely independent of the grid orientations and which possess self-validating capabilities. 3) It may also be necessary to show that compliance is achieved despite manufacturing variations.

In contrast, an accurate and highly sensitive measurement setup would allow tests of randomly selected samples of a product whereas no modelling or alteration of the product being investigated would be necessary. The position of the device would be easily modified when seeking the worst case conditions. An important difference to numerical simulations is that only the system (including phantom) and not each measurement must be validated. As the location of the strongly local maximum is not known *a priori*, the SAR distribution in a larger volume of the exposed tissue must be scanned, requiring a large degree of mobility of the probe within the tissue. This in turn, restricts the possible complexity of the phantom.

This paper presents a system that enables the automated measurement of the absorption distribution as well as the assessment of the spatial peak SAR values inside any tissue simulating solution.

II. Laboratory Setup

The SAR can be determined by measuring either the electric field (E) or the temperature rise ($\delta T/\delta t$) inside the exposed tissue

$$SAR = \frac{\sigma}{\rho}E^2 = c\frac{\partial T}{\partial t} \tag{1}$$

where σ is the conductivity, ρ the density and c the specific thermal constant of the tissue at the site of measurement.

In the setup shown in Fig. 1, the SAR distribution is determined by measuring the electric field with miniaturized E-field probes. Measuring the temperature rise in the simulated tissue does not provide sufficient sensitivity for compliance testing of consumer products [11]. However, this technique is used for the validation of the system as well as for the calibration of the probes (see Section VIII).

Measurements are done in shell phantoms filled with tissue simulating solution. In the laboratory three types of shell phantoms are used:

1) Geometrically simple phantoms for calibration and numerical validation of the system.
2) Simplified body and head phantoms to simulate worst-case conditions of exposure with real devices.
3) Very detailed phantoms to investigate the effects of different tissue layers (skin, living bone, air cavities, etc.), different exposure conditions (device positions, hand effect, spectacle frames, etc.) and to validate the simplified phantoms.

The E-field probes are positioned by a 6-axis precision robot (Stäubli RX90) inside shell phantoms with a working range greater than 0.9 m and with a position repeatability

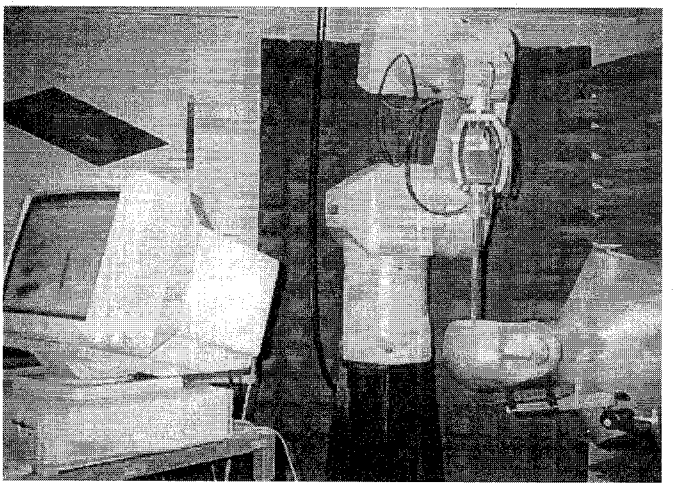

Fig. 1. Laboratory setup inducing robot, probe, data acquisition electronics, phantom, and PC.

that is better than ± 0.02 mm (at constant temperature). Each probe incorporates an optical surface-detecting systems, which permits the accurate positioning of the probe with respect to the phantom's surface. Basically the SAR with respect to the phantom's surface. Basically the SAR distribution in any volume can be measured. The currently implemented compliance test involves first measuring the SAR on a coarse 3-D-grid in a preselected volume. Afterwards a fine 3-D-grid around the previously detected maximum is measured. The 1g or 10g-average SAR-values are interpolated from the fine-grid results. The procedure is completely automated and takes less then 15 minutes, which is well within the battery lifetime of standard communication devices.

III. Isotropic E-Field Probes

The most crucial components of the whole system are the E-field probes. The main requirements are:

1) High sensitivity and linear response over a broad frequency range.
2) High spatial resolution.
3) Isotropy in differing media.
4) Low interaction with the measured field.
5) Small size.

For optimal performance under different measuring conditions, two types of E-field probes have been developed. The design with the triangular core (Fig. 2) was selected for dosimetric measurements in liquids with high permittivity because of the smaller outline and the possibility of placing the surface detector in the center of the probe. The "rectangular" design (Fig. 2) with one dipole parallel to the probe axis enables the separation of the field vector components corresponding to the coordinates of the probes, i.e., parallel and normal to the probe axis. This results in better omnidirectivity, especially in low-epsilon media [16]. However, the probe has an asymmetric core and a slightly bigger profile.

Each probe consists of three small dipoles (3mm) directly loaded with a Schottky diode and connected with resistive lines to the data acquisition unit. The theory of this type of probe

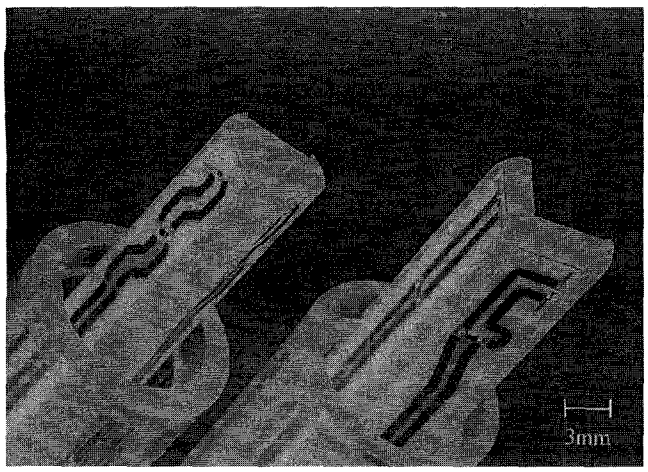

Fig. 2. Tips of the "triangular" (left) and the "rectangular" (right) probes. The tip shell has been removed.

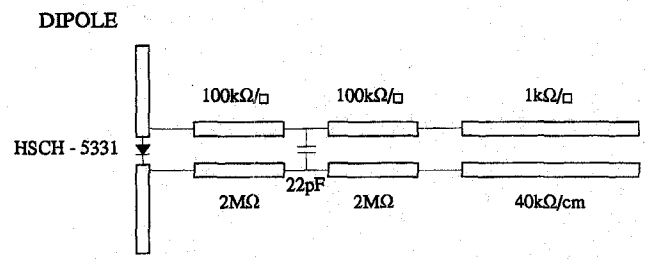

Fig. 3. Equivalent circuit representation of the probe.

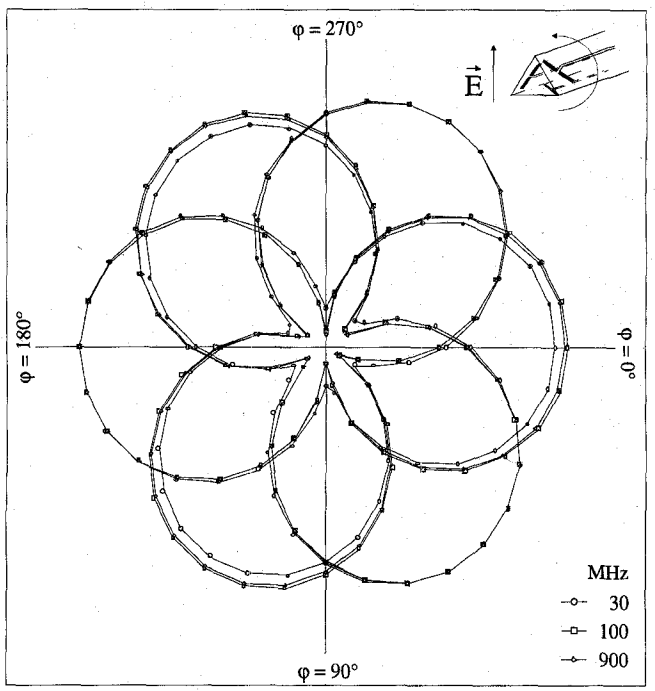

Fig. 4. Directivity diagram of the new probe in thick-film technique with the E-field normal to the probe axis. Measured using the TEM cell (ifi110) between 10 MHz and 900 MHz.

has been discussed previously in various publications (e.g., in [17]). While these papers describe the probe's characteristics by modelling the components (dipole-diode-line), they do not discuss the influence of the dielectric supporting materials of the probe, which can completely distort the theoretical dipole-characteristics. To further improve the directivity of the probes, special attention has been paid to these constructional problems.

A. Problem 1: Secondary Modes of Reception

An important part of most antenna design is to suppress secondary reception modes produced by the connecting lines, constructional asymmetries, etc. In the probes described above there are several possible secondary reception modes. One is produced by normal mode signals coupled into the resistive lines and rectified in the diode. These signals can be reduced by decreasing the spacing between the lines or by filtering techniques. Another mode is produced by common mode signals coupled into the lines and converted at the diode into normal mode signals by asymmetrical loading of the dipole halves due to constructional asymmetries (especially when measuring in the immediate proximity of metallic structures). As the source impedances of these modes have high resistive components, they are negligible at higher frequencies where the (mainly capacitive) impedances of the antenna and diode are much lower. At lower frequencies, however, these modes can become dominant and distort the ideal antenna characteristics (see Fig. 5).

Other electromagnetic fields present in the laboratory can also be the source of such secondary signals, especially ELF fields produced by power lines or robot control signals. A carefully designed laboratory grounding system has proven to be of great importance for high probe sensitivity.

In order to suppress these modes and make the probe useful for frequencies down to 10 MHz, a distributed filter was introduced between the dipole and the resistive line (see Fig. 3).

The thick-film technique was employed for the construction of the dipole and lines instead of the normally used thin-film technique. This permits the use of lines with different sheet resistances on the same substrate, and the production of much higher sheet resistances than manufacturable with the thin-film technique. Since the thick film layers are printed using silk screening, the structures are much coarser than those of thin-film probes.

In Fig. 4 the directivity diagram normal to the probe axis of the "triangular" probe is shown between 10 MHz and 900 MHz. For comparison, Fig. 5 shows the same diagram of the well-known E-field probe in thin film technology (50 μm line spacing and width) described in [17]. Apparently, the performance degeneration caused by direct coupling effects between dipole and line (TEM cell ifi110) could be significantly reduced by this new approach.

The high resistive decoupling of the diode from the detector circuit has another desired effect. The diode impedance has less influence on the timing characteristic of the detector circuit. This prevents the usual "peak detector characteristic" of diode detector probes for pulsed signals. In Fig. 13, the rms response of this approach is tested for duty cycles of up to 100.

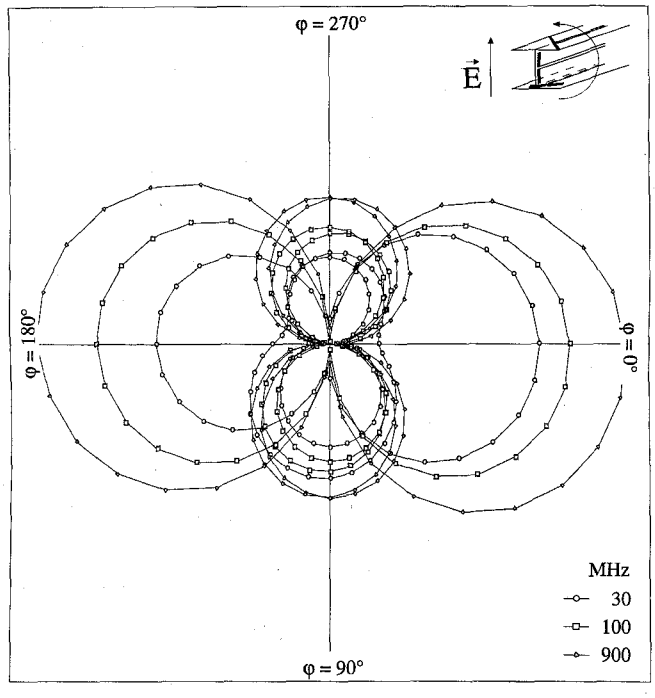

Fig. 5. Directivity diagram of the standard probe in thin-film technique with the E-field normal to the probe's axis. Measured using the TEM cell between 10 MHz and 900 MHz.

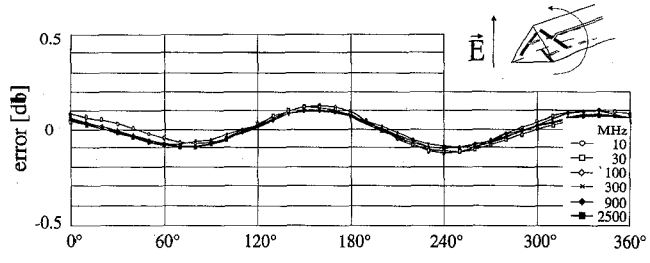

Fig. 6. Deviation from isotropy of the probe with triangular design in air, whereby the E-field was rotated in a plane normal to the probe axis. Measured using the TEM cell (ifi110) between 10 MHz and 900 MHz and the waveguide R26 at 2500 MHz.

B. Problem 2: Influence of the Probe Materials on the Field

Any dielectric material around electric dipoles will have an effect on the local signal strength. It is obvious from the construction of these probes that the influence on E-field components normal to the probe axis will be different to those on E-field components parallel to the probe axis. Furthermore, this difference in sensitivity depends on the surrounding media. This results in poor isotropy in planes that include the probe axis.

Figs. 6 and 7 show the deviation from isotropy of the probe with triangular design in air and brain simulating solution in a plane normal to the probe axis and in a plane through the probe axis, respectively.

It can be clearly seen that the component of the E-field in the direction of the probe axis in air is much stronger than the component normal to the probe axis, while in solutions with high permittivity this effect is reversed, but to a much lesser extent. While this probe works well in solutions which

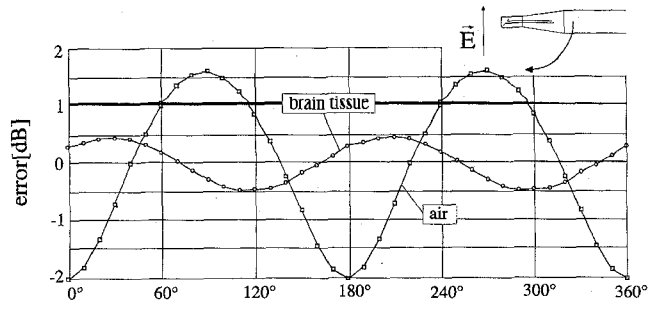

Fig. 7. Deviation from isotropy of the probe with triangular design in air at 2500 MHz (above an open waveguide R26) and in brain tissue equivalent solution (900 MHz), whereas the E-field was rotated in a plane through the probe axis.

simulate the electric properties of tissues with high water content, it proves to be unusable in air (unless the polarization of the E-field is known in advance and the probe placed accordingly, i.e., normal to the field). This problem can be overcome in the following ways:

1) By selecting material for construction with the same characteristics as the surrounding media. As such material must be easily mechanically processible, no such materials for air or for biological tissue are available.
2) By adjusting the angular orientation of the dipoles in order to compensate for the different sensitivities along and normal to the probe axis. It follows that such a probe would only be usable in a single surrounding media.
3) Another approach is to compensate for these effects by numerically weighting the dipole-signal input according to the field orientation with respect to the probe extension. This is only possible if the component of the E-field along the probe axis can be separated, i.e., if one of the probe's dipoles is aligned along the probe axis. This has been successfully accomplished in the "rectangular" design which is described in [16] (see also Fig. 2). By simply introducing a media-dependent conversion factor for the signal of the component along the probe axis, the isotropy in air is better than ±0.5 dB in all directions and for all polarizations.

The probe with the triangular design was selected for dosimetric measurements for the following reasons:

1) There was slightly better isotropy in planes normal to the probe axis due to the high degree of constructional symmetry in this plane.
2) The slightly weaker isotropy in the other planes in solutions with high water content is not a significant drawback. The reason being that the components of the E-field along the probe axis, i.e., normal to the phantom surface, have been shown to be significantly smaller than components in other directions. This has been predicted in [2] and is demonstrated in Figs. 8 and 9. Hence, the maximum error introduced by this lack of isotropy is much less than the deviation of ±0.6 dB in Fig. 7.
3) The fact that the dipole orientation differs from the probe orientation is not a disadvantage because only the total field is of interest in dosimetric applications.

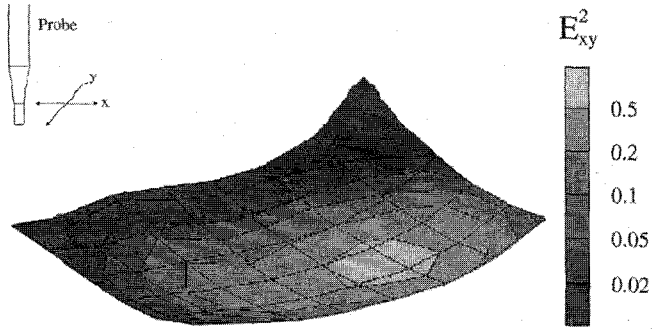

Fig. 8. Distribution of the SAR component normal to the probe axis in the shell phantom measured with a commercial mobile phone.

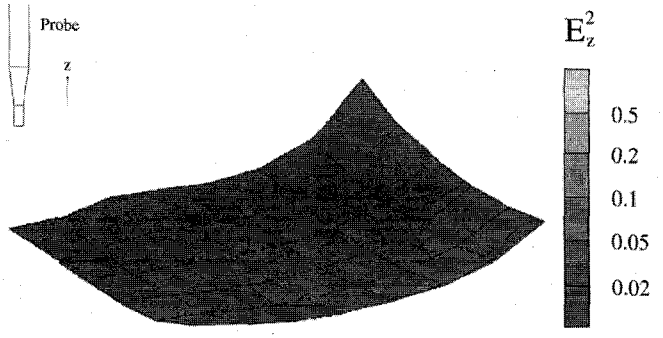

Fig. 9. Distribution of the SAR component in the shell phantom parallel to the probe axis measured with a commercial mobile phone.

4) The high degree of constructional symmetry improves the efficiency of the described filtering method for secondary reception modes. The frequency response at frequencies below 100 MHz is better than in the probe with the "rectangular" design.
5) The triangular design is very compact and ensures a high spatial resolution. The distance between the dipole centers is less than 2 mm.
6) The surface detection system (see Section V) is positioned in the center of the probe. This ensures excellent positioning accuracy even when the probe is not normal to the phantom surface.

C. Problem 3: Influence of the Probe on Inhomogeneous Fields

The disturbance caused by the probe on inhomogeneous fields depends not only on the probe material and geometry but also largely on the field itself. The influence of these effects must be investigated in each case. Fig. 14 shows the results of SAR measurements in brain simulating solution near the shell of the phantom.

If the distance between the probe tip and surface of the phantom is less than 1 mm, the field distribution inside the probe tip differs due to short circuiting between the probe and the outside media, i.e., the measured values become too high. This error source is greater than the error caused due to scattering effects by the probe at the interface [18]. The problem can be solved by measuring the SAR at different distances from the surface and extrapolating the SAR values to the surface. (This extrapolation procedure is also necessary because of the separation of the dipole center from the probe tip.)

Another source of error in inhomogeneous fields arises from the spacing between the dipole centers in the probe. Because each field component is measured at a slightly different location, discrepancies are to be expected where field magnitudes or directions change rapidly within the probe's dimensions. Because of the nature of the absorption mechanism [2], the field gradients induced by mobile phones operating at frequencies below 3 GHz have larger dimensions that the probe's diameter.

IV. Probe Construction

The probe consists of a two-shell construction. The core which holds the ceramic substrate is made entirely of the synthetic microwave material (STYCAST 0005) with a permittivity of 2.54 and a loss tangent of 0.0005. The tip of the outer shell is made of the same material and the main outer shell is made of common PMMA tubing. The core is centered at the tip and held in place with a spring at the connector end. A slight deformation of the outer shell does not effect the fragile core. The probe can be dismantled for repair. Between the core and the outer shell, a sheet of very high resistivity is introduced to neutralize static charges on the exterior of the probe or in the measuring setup. The distance between the probe tip and the dipole center is 2.7 mm.

The probe is connected with a precision 7-terminal connector to the acquisition unit. The counter part in the acquisition unit is flexibly mounted. If excess force is applied to the probe, the probe will give way and a touch detection logic in the acquisition unit will immediately stop the robot. A dielectric tube over the probe connector holds the probe flexibly at a second point 8 cm from the connector. This ensures very high accuracy in the positioning of the probe tip at all probe angles.

V. Surface Detection

The surface detection system included in the probes consists of an optical multifiber line. Half of the fibers are pulsed by an infrared LED, the other half are connected to a synchronized receiver. An object in the correlation area of the two fiber ends causes a coupling between transmitting and receiving fibers. When the probe is moved towards the surface, the reflected signal increases until it reaches a maximum approximately 1.2 mm from the surface, from where it decreases until the probe touches the surface. The location of the maximum is independent of the surface reflectivity and largely independent of the angle between the probe and the surface (see Fig. 10). The complete setup gives a positioning accuracy of the probe with respect to the surface of ± 0.2 mm.

VI. Data Acquisition Electronics

The improved probe characteristics were obtained at the cost of increased demands on the signal amplifier. The probes have source impedances of 5 to 8 MΩ due to the high resistive lines and the decoupling filters. The rectified signals range from 1 μV to 200 mV. High noise signals (especially induced signals from power lines) are to be expected.

The first unit of the data acquisition system is housed in a metal box of dimensions 68 $\times$ 57 $\times$ 46 mm, is battery

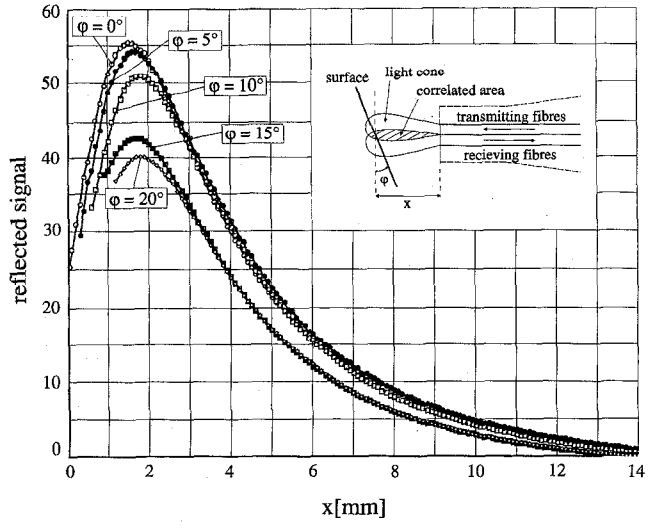

Fig. 10. Response of the surface detector as a function of the distance (×) from the surface.

powered and is connected with fiber-optic links to the main data evaluation system. The system can therefore be used in situations where telemetric measurements are necessary.

Fig. 11 shows the block diagram of the data acquisition system.

1) Pulse relays with low thermal voltage (<0.5 μV) for offset calibration.
2) Input filter to prevent HF-signals passing to the amplifier and being rectified in input nonlinearities.
3) Electrometer grade differential input amplifier (<0.1 pA bias current).
4) Second stage instrumentation amplifier with $\times 1/\times 100$ gain.
5) Multiplexer to switch between channels and gain.
6) Fast 16–bit sampling AD-converter with serial output.
7) Control logic for power down mode, calibration cycle, channel selection, gain selection.
8) Touch logic with asynchronous transmission of touch state signal to instantly stop the robot's movement.
9) Optical up-link with 1 MHz clock, synchronization and control signals.
10) Optical down-link with serial data and state signals (low battery, touch, channel address, etc.).
11) Rechargable battery pack for five hours of operation.
12) Computer plug-in card with main timing unit, data conversion of the serial E-field data and state signals, data acquisition of the analog signal from the surface detection amplifier and fast digital link to the robot.
13) Optical transmitter/receiver for the surface detection system.

VII. Software

For ease and speed of measurements, a program has been written in C^{++} under Windows, to perform all involved tasks: Data acquisition, surface detection, robot control, administration of all calibration parameters of the system, evaluation and visualization of the measured data. Complex measuring tasks are available at the push of a button.

A. Robot Control

The robot is completely controlled by the PC and its movements can be monitored on the screen. Some program modules are downloaded to the robot computer for faster response times.

Several measuring options permit complete measurements in user defined volumes, planes or along lines with or without surface detection. The measuring process is displayed on the screen. The filtered raw data from the data acquisition system is stored in data files together with all the calibration parameters. If a measurement is made with false parameters, it is possible to correct the parameters in the file and reevaluate the data.

B. Data Processing

The data acquisition system samples 7800 data sets per second, i.e., 2600 complete field measurements per second for 3-D probes. The program reads and filters the incoming data during the measuring or surface detection cycles. Depending on the received signal strength, the program switches the gain of the amplifier unit and launches calibration cycles accordingly. The program calculates an accuracy estimate of the filtered signal and stops the measuring cycle upon reaching the desired accuracy. The measuring time per grid point (always a multiple of the power line period) varies with the desired accuracy and the received signal-to-noise ratio.

Fig. 12 shows the deviation from linearity in function of the signal strength in V/m and the equivalent SAR values for brain tissue. The line with the empty symbols show the values before and those with the dark symbols those after numerical compensation of the diode compression. For low signal strengths, the measuring time was 10 seconds, for stronger signals 1 second.

Because of the low cutoff frequency the system cannot follow pulsed HF signals, but provides an average value of the rectified signal. As long as the signal strength stays within the square law range of the detector diode, the reading is the average of the absorbed power. If the peak signal strength is higher, the compression of the diode must be compensated. This is done automatically by the evaluation software depending on the duty cycle parameter. The system then calculates the peak power, compensates for the diode compression and gives the new average value.

Fig. 13 shows the measured error between CW and pulsed signals with pulse frequencies between 10 Hz and 1 kHz and duty cycle between 1 and 100.

C. Data Visualization

The program evaluates the raw data with the calibration parameters and can produce two-dimensional or three-dimensional graphical output with interpolated isolines in different units (μV of rectified signal, V/m, SAR, power flow density, etc.). The total field strength of each of the dipole components can be separately plotted. SAR values can be

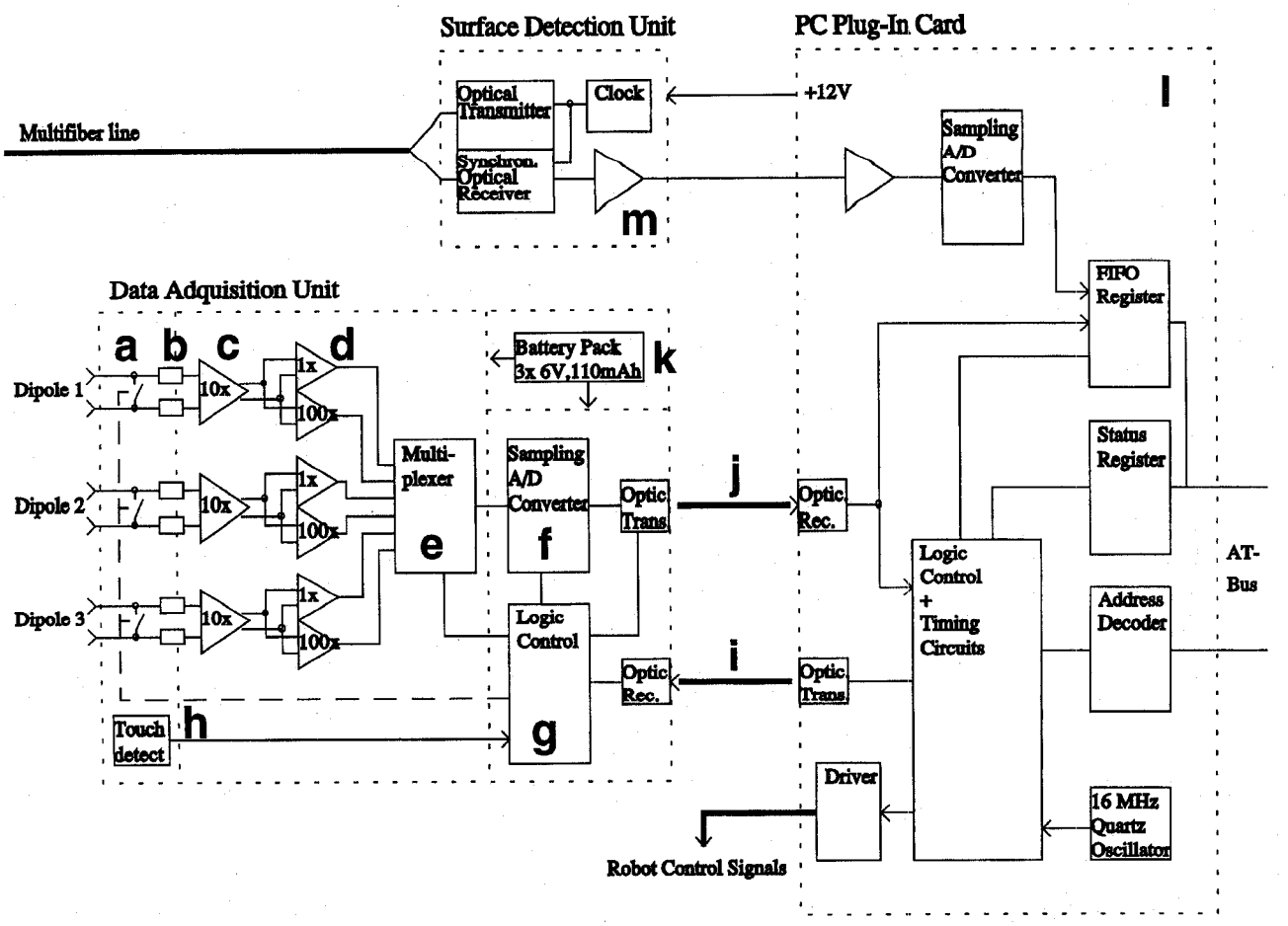

Fig. 11. Block diagram of the data acquisition hardware.

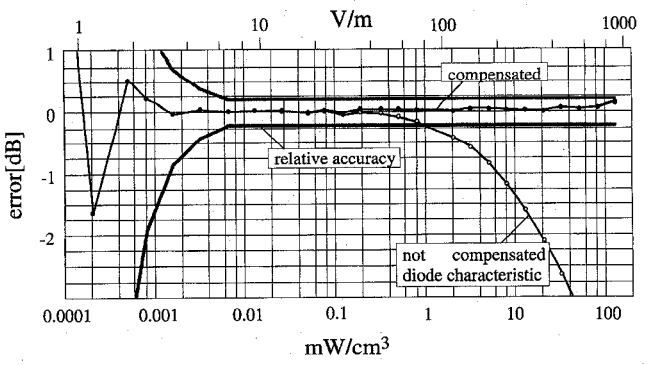

Fig. 12. Deviation from linearity. The line with the dark symbols are the values after compensation of the diode compression. The data was obtained from measurement at 900 MHz in the TEM cell (ifi 110).

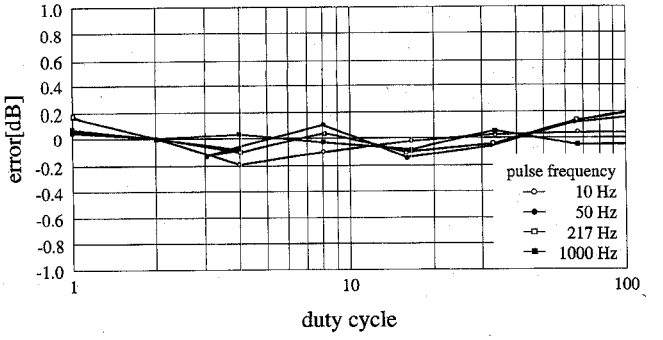

Fig. 13. Measured error between CW and pulsed signals with pulse frequencies between 10 Hz and 1 kHz and duty cycle between 1 and 100. Reference was a HP437B peak power meter.

numerically integrated over 1 g or 10 g of simulated tissue. Evaluated data can be exported to other file formats. Figs. 8 and 9 demonstrate one of the various implemented graphical visualizations.

VIII. Calibration and Validation of the System

The system can be easily calibrated for air in known fields (far field of antennas or in TEM cells and wave guides). In solutions, however, a conversion factor must be introduced to account for the different sensitivities of the probes in the solution. This conversion factor was obtained by comparing the measured values with those from numerical simulations. The simple setup was already used in [2] and consists of a standard half wave dipole below a half-plane phantom.

To validate the result, the same setup was used with a 100 W amplifier and temperature measuring equipment. The fiber optical temperature probes have a diameter of less than 0.5 mm allowing true point measurements. However, high power is required because of the rather low sensitivity (>10 mW/g).

TABLE I
SYSTEM SPECIFICATIONS WITH ISOTROPIC E-FIELD

frequency range	10 MHz to > 3 GHz
dynamic range in tissue simulating solutions	1 μW/g to 100 mW/g
linearity	< ±0.2 dB
deviation from isotropy in tissue(triangular probe)	
- normal to probe axis	± 0.2 dB probe.
- in all planes, all polarizations	± 0.8 dB
variation with frequency	< ± 0.2 dB
spatial resolution of SAR measurements	< 0.125 cm^3
reproducibility of probe positioning	< ± 0.2mm

Note: The rather large deviation from isotropy in all planes scarcely affects the accuracy of dosimetric assessments if the probe is positioned predominantely normal to the phantom surface.

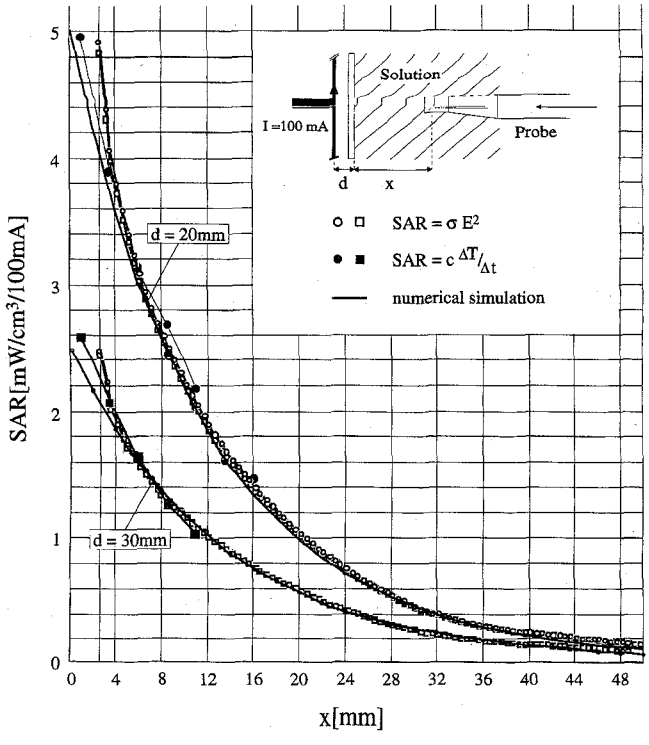

Fig. 14. Comparison of SAR values obtained by numerical simulation, measured temperature rise and E-field measurements for the same setup (plane phantom exposed to a half wave 900 MHz dipole parallel to the phantom's surface). The phantom was filled with brain equivalent solution ($\epsilon_r = 44$, $\sigma = 1.1$ mho/m). All values are normalized to an antenna feedpoint current of 100 mA.

Fig. 14 shows the results of the three evaluation methods at different distances from the transmitting dipole and the probe from the bottom of the phantom.

IX. CONCLUSION

The developed measurement system is a flexible, automated, time-efficient tool to assess SAR distributions in tissue simulating solutions. It is especially suited for compliance testing of handheld or body mounted devices with specific safety standards. Tests have shown an excellent reproducibility of the integrated peak SAR values of well within ±5% even when changing the starting measuring grid. The specifications of the system can be summarized as in Table I.

Although the main emphasis is now on the open phantom issue, several improvements are anticipated. For instance, extension of the system for general near field measurements used in antenna design, EMI, EMC.

ACKNOWLEDGMENT

The development of this scanning system was supported by the Federal Ministry of Posts and Telecommunications (Germany), Deutsche Telekom (Germany), Swiss Telecom PTT (Switzerland) and Mannesmann GmbH (Germany). The authors gratefully acknowledge the help of K. Meier, M. Schmid, J. de Keijzer, as well as valuable advice of Dr. Q. Balzano and O. Garay.

REFERENCES

[1] R. F. Cleveland and W. T. Athey, "Specific absorption rate (SAR) in models of the human head exposed to hand-held UHF portable radios," *Bioelectromagnetics,* vol. 10, no. 1, pp. 173–186, Jan. 1989.

[2] N. Kuster and Q. Balzano, "Energy absorption mechanism by biological bodies in the near field of dipole antennas above 300 MHz," *IEEE Trans. Veh. Technol.,* vol. 41, no. 1, pp. 17–23, Feb. 1992.

[3] ANSI/IEEE C95.1-1991, *IEEE Standard for Safety Levels with Respect to Human Exposure to Radio Frequency Electromagetic Fields, 3 kHz to 300 GHz,* The Institute of Electrical and Electronics Engineers, Inc., New York, NY 10017, 1992.

[4] CENELEC CLC/SC111B, *Draft European Prestandard (prENV 50166-2, Human Exposure to Electromagnetic Fields High-Frequency: 10 kHz–300 GHz.* CENELEC: Brussels, 1993, Draft, Sept., 1994.

[5] N. Kuster, "Multiple multipole method for simulating EM problems involving biological bodies," *IEEE Trans. Biomed. Eng.,* vol. 40, no. 7, pp. 611–620, July 1993.

[6] ——, "Multiple multipole method applied to an exposure safety study," in *ACES Special Issue on Bioelectromagnetic Computations,* A. H. J. Fleming and K. H. Joyner, Eds., vol. 7, pp. 43–60. Applied Computational Electromagnetics Society, no. 2, 1992.

[7] P. J. Dimbylow, "Finite-difference time-domain calculations of SAR in a realistic heterogeneous model of the head of planewave exposure from 600 MHz to 3 GHz," *Phys. Med. Biol.,* vol. 38, no. 12, pp. 361–368, 1993.

[8] N. Kuster, T. Schmid, and K. Meier, "Untersuchungen der Absorption im extremen Nahfeld von Sendern," in *VDE-Fachbericht 45: Biologische Wirkungen elektromagnetischer Felder,* Verband Deutscher Elektrotechniker (VDE), Nov. 1993, pp. 135–143.

[9] O. P. Gandhi, J.-Y. Chen, and D. Wu, "Electromagnetic absorption in the human head for cellular telephones," in *Proc. 14th Ann. Meet. of Bioelectromagnetic Soc.,* Copenhagen, Denmark, June 1994.

[10] P. J. Dimbylow and S. M. Mann, "SAR calculations in an anatomically realistic model of the head for mobile communication transceivers at 900 MHz 1.8 CHz," *Phys. Med. Biol.,* vol. 39, no. 12, pp. 1537–1553, 1994.

[11] K. Meier, O. Egger, T. Schmid, and N. Kuster, "Dosimetric laboratory for mobile communication," in *Proc. 9th Symp. on Electromagnetic Compatibility,* Zürich Mar. 1995.

[12] A. H. J. Fleming, "A numerical estimate of SAR levels in a heterogeneous model of the head due to exposure by a mobile phone," in *Proc. of the 14th Ann. Meet. Bioelectromagnetic Soci.,* Copenhagen, Denmark, June 1994.
[13] M. A. Jensen and Y. Rahmat-Samii, "EM interaction of handset antennas and a human in personal communications," *Proc. IEEE,* vol. 83, no. 1, pp. 7–17, Jan. 1995.
[14] Strahlenschutzkommission, "Empfehlung der Strahlenschutzkommission verabschiedet auf der 107. Sitzung am 12./13. Dezember 1991," in *Schutz vor elektromagnetischer Strahlung beim Mobilfunk,* SSK, Ed. Gustav Fischer Verlag, 1992, pp. 3–18.
[15] Federal Communication Commission, "Amendment of the commission's rules to establish new personal communication services," Tech. Rep. FCC 94-144, FCC, Washington, D.C. 20554, 1994.
[16] T. Schmid and N. Kuster, "Novel E-field probes for close-near field scanning," *IEEE Trans. Veh. Technol.,* submitted.
[17] H. I. Bassen and G. S. Smith, "Electric field probes—a review," *IEEE Trans. Antennas Propagat.,* vol. 31, no. 5, pp. 710–718, Sept. 1983.
[18] G. S. Smith, "The E-field probe near a material interface with application to the probing of fields in biological bodies," *IEEE Trans. Microwave Theory Tech.,* vol. 27, no. 3, pp. 270–278, Mar. 1979.

Thomas Schmid worked from 1984 to 1987 at the Swiss Federal Institute of Technology in Zurich. He was involved in research into medical applications of microwaves and electroacoustic wave propagation in crystals. From 1988 to 1992 he worked for the OIM (Oranisacion Intergubernamental de Migraciones, Geneva) where he was involved in technical and educational development projects for Central America. During this time he served as Professor at the Universidad National de Ingeniería (UNI) in Managua, Nicaragua and founded as an independent enterprise a service-center (UNITRON) at the University for state institutions and industries. In 1990 he was responsible for the technical setup of the general elections in Nicaragua. In 1993 he joined the Laboratory for Electromagnetic Fields and Microwave Electronics, ETH, where he has been developing near field probes and the dosimetric assessment system DASY. In late 1994, he cofounded the spin-off company Schmid & Partner Engineering AG.

Oliver Egger was born in Doncaster, UK, in December 1971. He is currently studying computer science in the final year at the Swiss Federal Institute of Technology (ETH), Zurich, Switzerland.

He has been working at the Electromagnetics Laboratory (ETH) since July 1993, where he was responsible for programming the software for the dosimetric assessment system (DASY2)

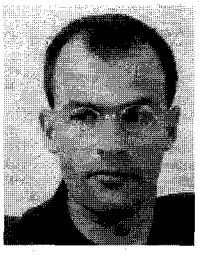

Niels Kuster was born in Olten, Switzerland in June 1957. He received the Diploma and Ph.D. degrees in electrical engineering from the Swiss Federal Institute of Technology (ETH) in Zurich.

He joined the Electromagnetics Laboratory at ETH in 1985 where he was involved in the research and development of the Generalized Multipole Technique (GMT) and the 3D MMP code. In 1992 he was invited Professor at Motorola Inc. in Fort Lauderdale, FL for a trimester. He currently is Assistant Professor at the Department of Electrical Engineering, ETH Zurich. His research interests include all aspects of numerical methods in electrodynamics, antenna design and bioelectromagnetics.

Dr. Kuster is a member of various scientific societies and official member of URSI Commission K.